Evolutions towards a new LSPR particle: Nano-sinusoid

Progress In Electromagnetics Research, Vol. 132, 199–213, 2012

EVOLUTION TOWARDS A NEW LSPR PARTICLE: NANO-SINUSOID

D. Mortazavi[1, *], A. Z. Kouzani[1], and L. Matekovits[2]

[1]School of Engineering, Deakin University, Geelong, VIC 3216, Australia

[2]Dipartimento di Elettronica e Telecomunicazioni, Politecnico di Torino, Italy

Abstract—This paper proposes a novel nano-sinusoid particle to be employed in enhanced localized surface plasmon resonance (LSPR) bio-sensing devices. Numerical investigations are carried out to demonstrate advantages offered by the proposed nano-particle on LSPR enhancement over other nano-particles including noble nano-triangles and nano-diamonds. Although nano-triangles exhibit high concentration of the electric field near their tips, when illuminated with a light polarized along the tip axis, they present only one hot spot at the vertex along the polarization direction. To create a structure with two hot spots, which is desired in bio-sensing applications, two nano-triangles can be put back-to-back. Therefore, a nano-diamond particle is obtained which exhibits two hot spots and presents higher enhancements than nano-triangles for the same resonant wavelength. The main drawback of the nano-diamonds is the fluctuation in their physical size-plasmon spectrum relationships, due to a high level of singularity as the result of their four sharp tip points. The proposed nano-sinusoid overcomes this disadvantage while maintaining the benefits of having two hot spots and high enhancements.

1. INTRODUCTION

Biosensors operate according to the measurement of the scattered wave from biomolecules, e.g., protein detection SERS biosensors [1] and ultra sensitive tunable optical sensors [2]. Since the scattered wave is usually very weak for detection, the incident field needs to be magnified. Metal nano-particles (NPs) have been used to magnify

Received 11 August 2012, Accepted 21 September 2012, Scheduled 27 September 2012

* Corresponding author: Daryoush Mortazavi (daryoush.mortazavi@gmail.com).

the incident field. Once the incident field is locally increased, it is beamed toward the target molecules. This process, which is called surface enhanced Raman scattering (SERS), enhances the amplitude of the Raman scattered wave from the target molecules [3]. When the collective resonance of valence electrons in the noble metal is equal to the frequency of the incident light, dipolar localized surface plasmon resonance (LSPR) is generated [4, 5], where the incident wave may excite dipolar LSPRs on the surface of the noble metal NPs. The nano-plasmonic phenomenon happens when (i) the NP permittivity is a complex function of frequency where its real part is negative in some frequency values in negative index materials (NIM), and (ii) the free-space wavelength is large with respect to the NP dimensions; these two conditions only occur simultaneously at nano-scale geometries of noble metals, such as silver and gold, when they are illuminated at frequencies in the visible range [6]. Plasmon resonances have been experimentally investigated in metal self-assembled quantum dots [7, 8] and in nanoparticles of complex shapes [9, 10] by means of different techniques.

In addition to the aforementioned dipolar resonances, higher modes of plasmon excitation can also occur when the angular momentum l is larger than unity; such an example is the quadrupole mode ($l = 2$), where half of the electron cloud moves parallel to the applied field, and the other half moves anti-parallel to the applied field [4].

The electromagnetic field is singular near discontinuities. When a resonator geometries present some discontinuities, i.e., hot spots, the surface charges generated by an incident electromagnetic field is highly concentrated near these points. The presence of such high field spots is desired when the intensity of the field is too small to be accurately measured. An example of using hot spots is the SERS, where the field is collected at the tip points. When dipoles are excited, the maximum enhancement occurs at the tip points, while quadrupole resonances are concentrated on plain sides, as shown for nano-stars [11]. Tip-surface is also utilized in tip-enhanced Raman spectroscopy (TERS) for the excitation of the LSPR as a scanning probe. TERS does not need any noble-metal substrates; using silver tips in the TERS, enhancements of up to 10^{14} fold in the Raman signal have been claimed [12]. Nowadays, the applications of nano-particles have been extended to meta-material (MM) biosensors [13]. Moreover, an Au/Ag alloyed triangular nano-box (TNB) device has recently been used as a multifunction device in SERS biosensing and in-vivo cancer drug delivery, where the femtosecond laser pulses are used to ablate the TNB and release the drug encapsulated in the TNB hollow [14].

In this paper, the effect of sharp points on the LSPR spectrum for NPs such as nano-triangles and nano-diamonds are first investigated. Inspired by the shape and features of nano-diamonds, a new nano-sinusoid shape is proposed, which exhibits more linear plasmon wavelength-size relationship than nano-triangles and nano-diamonds. Similar to nano-diamonds, the proposed shape gives high electric field enhancements, and the presence of the two hot spots makes the particle suitable for applications such as SERS biosensing. Finally, the effects of the size and the elongation of the three types of NPs on the plasmon spectrum is investigated and compared.

2. THEORETICAL BACKGROUND

2.1. Arbitrary Shape NPs

Assume that a metal nano-spheroid with permittivity ε_m is embedded in a medium of permittivity ε_d. The nano-spheroid is assumed to have a major axis of $2b$ and a minor axis of $2a$. When an electric field $\mathbf{E}_0$, which is polarized along the major axis, strikes the NP, the Raman enhancement factor is given by [15]:

$$g = (\varepsilon_m - \varepsilon_d)/(\varepsilon_m + \chi\varepsilon_d) \tag{1}$$

where χ is called the shape factor which is equal to 2 for a sphere. For prolate spheroids where $b > a$, χ is larger than 2, and for oblate spheroids where $b < a$, χ is less than 2. Due to the angular momentum $l = 1$, in the polarization direction along the major axis of the spheroid, a dipole resonance on the surface of the spheroid is generated. According to (1), the condition for realizing this resonance is $\mathrm{Re}\{\varepsilon_m + \chi\varepsilon_d\} = 0$. Therefore, in prolate spheroids ($\chi > 2$), the plasmon resonance red-shifts with respect to a sphere, because for longer wavelengths the real part of ε_m for metals is more negative, i.e., presents higher absolute value. However, in oblate spheroids ($\chi < 2$), the polarization of the incident field is normal to the symmetry axis of the spheroid, and consequently due to multipoles ($l \geq 2$), other resonances are generated. For a sphere ($\chi = 2$), the dipole resonance is generated when $\mathrm{Re}\{\varepsilon_m\} = -2\varepsilon_d$, and the quadrupoles ($l = 2$) are generated when $\mathrm{Re}\{\varepsilon_m\} = -1.5\varepsilon_d$ [16, 17].

Dipole resonance modes can be further investigated through the electrostatic eigenmode approximation. In this formulation, the surface plasmon resonances are calculated using the oscillating surface charge distribution (σ_r) at the surface denoted by the polar distance of $\mathbf{r}$ with surface the normal vector of $\hat{\mathbf{n}}$. For an arbitrary ensemble of NPs, the charge distributions can be written as a superposition of the

normal modes of each NP of the ensemble [18, 19] as follows:

$$\sigma(r) = \frac{\gamma}{2\pi} \oint \sigma(r_q) \frac{(r - r_q)}{|r - r_q|^3} \hat{n} dS_q \tag{2}$$

where γ, the eigenvalue or the natural resonance of a single NP due to the charges on the surface denoted by polar distance $\mathbf{r}_q$, is related to the plasmon resonant wavelength of the ensemble by:

$$\varepsilon_m(\lambda_r) = \varepsilon_d \frac{1 + \gamma}{1 - \gamma} \tag{3}$$

where λ_r is the peak wavelength of the surface plasmon resonance, $\varepsilon_m(\lambda_r)$ the permittivity of the metal at the resonant wavelength, and ε_d the permittivity of the background medium. For a single spherical element and in a limited range of sphere size, for nano-spheres in dipolar mode $\gamma = 3$ [18, 19]; therefore, (3) gives the resonant condition $\varepsilon_m(\lambda_r) = -2\varepsilon_d$ in a limited range of NP size. Practically γ is affected by multipoles, which causes smaller values. Therefore, this quantity must be substituted with its effective value γ_{eff}.

In the investigation presented below, on the inverse eigenvalue $1/\gamma$ for a single nano-sinusoid (introduced in the following section), there is almost a linear function of the size and the aspect ratio, while the same function for a nano-triangle and with more extent for a nano-diamond is very fluctuating. Since this parameter has been used for calculating the NPs interaction in the eigenmode interaction method in recent works [18, 19], such a linear variation allows both reducing the computational complexity of modeling, and increasing the accuracy due to fewer samples considered for the description of the interaction on a large frequency band. A more in-depth analysis of the influence of all parameters affecting the LSPR spectrum has recently been presented in [20–22].

2.2. Nano-sinusoid Shape NPs

A novel geometry is introduced to reduce some of the aforementioned drawbacks (nonlinearity and having just one hot spot) whilst maintaining the characteristics for a high sensibility sensing. The proposed geometry is similar to a diamond shape, but presents two important modifications with respect to it, that makes it suitable for the SERS biosensing. First, the transition from the symmetry axis towards the external part is changed from linear to exponential taper. It has been demonstrated that such a solution implicitly reduces impedance mismatch, hence the device incorporating such a solution exhibits a broader bandwidth. Second, the off-symmetrical tips are eliminated by smoothing the connection between the two arms.

Reducing the presence of discontinuity, the surface charge density will be lower, and there is the possibility to increase the level of charge density near the other existing tips positioned on the main symmetry axis of the molecule.

A combination of these two approaches gives rise to a sinusoid shape, which inherently exhibits a wide-band response [23, 24]. The resulting resonator is similar to a dipole of variable in-plane width, which in turn corresponds to different path length form one edge to the other. For a dipole of overall length L, the resonant frequency and resonant wavelength are given by:

$$f = c/2L\sqrt{\varepsilon_{eff}} \tag{4}$$

$$\lambda = 2L\sqrt{\varepsilon_{eff}} \tag{5}$$

where c is the speed of light in vacuum and ε_{eff} the effective dielectric constant of the NP. For the wide frequency band analysis, the value of ε_{eff} varies with frequency, making the analysis even more challenging.

For a rectangular cross section dipole ($a \times b$), equivalent radius can be computed and approximated as $r_{eff} = (a + b)/2$. The actual resonance (defined as the frequency where the imaginary part of the dipole input impedance is equal to zero) occurs at the length $L/\lambda = 0.47$. For the computation of the scattering cross section; however, it is common to specify the size of a particle of an arbitrary shape and volume in terms of an effective radius given by:

$$R_{eff} = (3V/4\pi)^{1/3} \tag{6}$$

where V is the volume of the nanoparticle. This approximation is valid if $\lambda \gg 2R$, which unfortunately does not hold for $w < 40\,\text{nm}$ in the visible range [25]; in this case, the absorption and scattering are dominated by higher order multipoles, and consequently the full Mie series should be considered. Mie and Gans have presented an analytical method to describe the extinction cross section of an ellipsoid metal nano-particle [26].

Equation (4) describes that the resonant frequency is inversely proportional to the length; hence one expects that a nonlinear variation of L, under given shape will reflect in a linear answer. On the other hand, contrary to a constant in-plane width printed dipole (or constant radii wire dipole), the in-plane width of the nano-sinusoid dipole varies smoothly (see Figure 1(c)), allowing the dipole to resonate for different frequencies. A similar behaviour can be observed for the diamond shape (Figure 1(b)), but the inverse of the linear transition corresponds to a function with a Fourier transform with higher electric field enhancement even far away from the spectral lines corresponding to the tips with respect to the proposed sinusoid shape

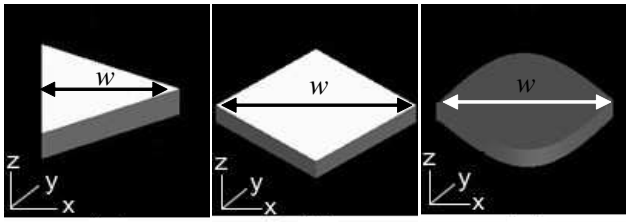

(a) (b) (c)

Figure 1. (a) Nano-triangle, (b) nano-diamond, and (c) nano-sinusoid topographies.

which will be smoother. Hence one expects that the eigenmodes of the novel resonator will exhibit a more linear behaviour for the sinusoidal shape. This observation is important, since the current distribution and the radiation pattern (also near-field) are related by the 2D Fourier transform. Furthermore, the substitution of the two off-symmetry tips with smooth transitions is expected to reflect in smoother spectra. The remaining discontinuities are along the symmetry axis, and will concentrate more surface charge, i.e., will increase the sensibility of the Raman scattering. A further feature of such geometry consists of the reduction of specular reflection of the surface current; therefore, reduction of the multi-resonances is expected. Moreover, the elimination of the two tips makes the structure also less sensitive to fabrication issues.

In particular, we have used the following expression to describe the proposed shape:

$$y = s(x) = \begin{cases} M \sin\left(\frac{x\pi}{w} - \frac{\pi}{2}\right) & \text{if} \quad -\frac{w}{2} < x < \frac{w}{2} \quad \text{and} \quad y > 0 \\ -M \sin\left(\frac{x\pi}{w} - \frac{\pi}{2}\right) & \text{if} \quad -\frac{w}{2} < x < \frac{w}{2} \quad \text{and} \quad y < 0 \end{cases} \tag{7}$$

where x is the actual in-plane width, M the modulation constant, y the actual position along the dipole main axis, and w the dipole overall length. Notation of the dipole in-plane width with s has been used in connection with its variable "slenderness ratio".

Considering our geometry, and differentiating Eq. (7) with respect to the longitudinal variable x, we have:

$$\frac{d}{dx} s(x) = M \frac{\pi}{w} \cos\left(\frac{\pi x}{w} - \frac{\pi}{2}\right) \tag{8}$$

In our case, $M = w/2$, and the tip is located at $x = w/2$, we have

$$\frac{d}{dx} s(x) = M \frac{\pi}{w} \cos\left(\frac{\pi x}{w} - \frac{\pi}{2}\right)\Big|_{x=\frac{w}{2}} = M \frac{\pi}{w} = \frac{\pi}{2} \tag{9}$$

Hence,

$$\frac{\theta}{2} = \text{atan}\left(\frac{\pi}{2}\right) = 57.51^\circ = 57.41\frac{\pi}{180} = 0.32\pi \tag{10}$$

As a result, the overall aperture of the tip is $\theta = 113.03^\circ = 0.638\pi$. According to the analysis in Ref. [27], the cutoff frequency ω_c can be calculated as:

$$\text{Re}\left\{\varepsilon(\omega_c)\right\} = \frac{\theta}{\theta - 2\pi} = -0.468 \tag{11}$$

Therefore, for silver nano-sinusoids the cutoff frequency is $\omega_c \approx 345\,\text{THz}$. At such vertex angle we conclude that (i) both the electric field and total Raman signal in a volume diverge, and (ii) the electric field is enlarged at the vertex, while the total Raman signal in a volume converges to a finite value. Since we are above the curve ω_c, the electric field will not vanish at the vertex. The cutoff frequency can be controlled by the modulation factor M, such that by decreasing M or by increasing the aspect ratio of the nano-sinusoids, a lower cutoff frequency is attained. All these characteristics correspond to our goal to increase the sensibility of the proposed NP. Consequently, the stated discussion also describes how to design the NP.

In the following section, a comparative study amongst triangle, diamond, and sinusoid NPs will be conducted and presented; also linearity of wavelength-size and enhancement of electric fields are demonstrated.

3. SIMULATION RESULTS AND DISCUSSION

Using the finite-difference time-domain (FDTD) method [28], the interaction of a source light (i.e., a total field scattered field (TFSF) source [28]) with a nano-triangle (Figure 1(a)), a nano-diamond (Figure 1(b)), and a new nano-sinusoid (Figure 1(c)) topographies are investigated in air, i.e., $\varepsilon_d = 1$. In this modeling, the substrate material is glass with refractive index of 3.81 and the NPs are silver which its permittivity is matched with a fourth order Drude-Lorentz model. Besides, all shapes have a z-oriented thickness of 30 nm. Silver is used as the NPs material because of its higher sensitivity than gold. However, silver NPs are subject to changes when exposed to water, acids, halides, and air. Therefore, silver NPs should be covered by a protecting layer for a long period [21, 29].

First, the single scatterers are illuminated by a plane wave propagating in the z-direction and with a polarization along the x-axis (0° polarization angle) over the optical wavelength from 300 to 950 nm. The extinction and scattering cross sections variations for various NP sizes have been observed. The considered excitation

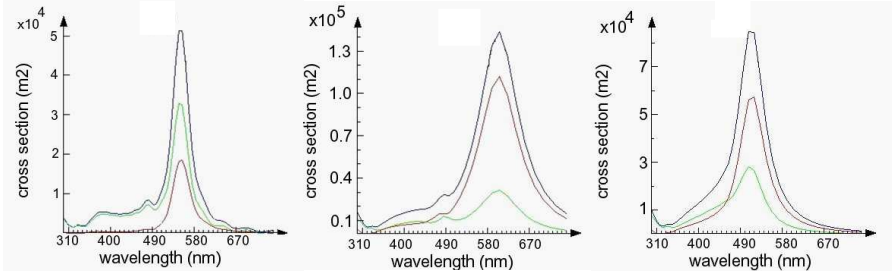

(a) (b) (c)

Figure 2. Extinction (blue), scattering (red), and absorption (green) cross sections for (a) silver nano-triangles of in-plane width 80 nm, (b) silver nano-diamonds of in-plane width 80 nm, and (c) silver nano-sinusoids of in-plane width 80 nm versus wavelength.

corresponds to illuminating the NPs along their elongation which has been theoretically proved in [16] to guarantee the maximum enhancement.

Figure 2 compares sample cross sections of silver nano-triangles of in-plane width $w = 80$ nm, nano-diamonds of in-plane width $w = 80$ nm, and nano-sinusoids of in-plane width $w = 80$ nm versus wavelength. The results demonstrate smoother LSPR spectrum of nano-sinusoids than nano-triangles and nano-diamonds, due to less multipoles excited in them. Simulation results for various NPs size also show that in nano-triangles with in-plane width less than 70 nm, nano-diamonds with in-plane width less than 60 nm, and nano-sinusoids with in-plane width less than 40 nm, the dipolar extinction and scattering cross sections are very low, and mostly multipoles are generated. Therefore, nano-sinusoids are better LSPR resonators in a wider size range with respect to nano-triangles and nano-diamonds. As seen in the figures, increasing the size of all considered NPs increases both the scattering and the extinction cross sections, and red-shifts the plasmon. These results are in line with the findings reported in [17, 30]. Also, it is obvious that the extinction and scattering cross sections of nano-sinusoids for in-plane width larger than 40 nm exclude any multipole resonances; however, multipole resonances are seen in the spectrum of nano-triangles and nano-diamonds even for sizes that are larger than 70 nm and 60 nm for nano-triangles and nano-diamonds, respectively.

Figure 3 compares the variations of the plasmon inverse eigenvalues and the plasmon wavelengths for the three considered NPs with respect to their size from 5–200 nm (i.e., the length of the symmetry axis along the x-axis for each NP); as expected, nano-triangles larger than 80 nm have an inverse eigenvalue-size relationship

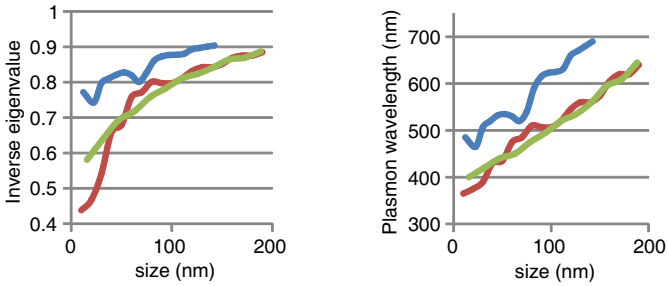

Figure 3. (a) Inverse of eigenvalue, and (b) plasmon wavelength for a silver nano-triangle (blue), a silver nano-diamond (red), and a silver nano-sinusoid (green), vs. size.

which is more linear than that for nano-diamonds; however, nano-diamonds cover a wider range of sizes but give more fluctuations in the spectrum due to its high level of singularity. Nano-sinusoids present a very linear relationship of inverse eigenvalue-size or plasmon wavelength-size, which makes them very suitable for fine tuning of the dipolar plasmon resonant wavelength whilst maintaining the dynamics of the nano-diamond geometry.

Therefore, using (3), the inverse eigenvalue γ_{eff} of nano-sinusoid NPs can be linearly approximated with respect to their in-plane width, and with a higher accuracy with respect to the other two considered NPs. As can be seen from Figure 3(a), nano-sinusoids inverse eigenvalues can be finely estimated by a straight line for in-plane width w larger than 40 nm via the following equation by a squared residual value of 0.9673:

$$\frac{1}{\gamma_{eff}} = 0.0014w + 0.6443 \quad \text{if} \quad w \geq 40\,\text{nm} \tag{12}$$

As a result, to have a significant dipolar resonance in nano-triangles, we need to increase their size to larger than 80 nm, but nano-sinusoids with sizes just larger than 40 nm are applicable. In addition, for the same ranges of size from 40 to 100 nm, nano-sinusoids generate wider ranges of plasmon wavelengths than nano-triangles associated with more linearity, as shown in Figure 3(b).

In addition, Figure 4 compares the variations of the plasmon extinction, scattering, and absorption cross sections for the three considered NPs with respect to their wavelength. The figure indicates less absorption cross section and more extinction and scattering cross sections in nano-sinusoids than nano-triangles and nano-diamonds, also more linearity of the cross sections versus wavelength for nano-sinusoids than the two other shapes. It can be noted that for above

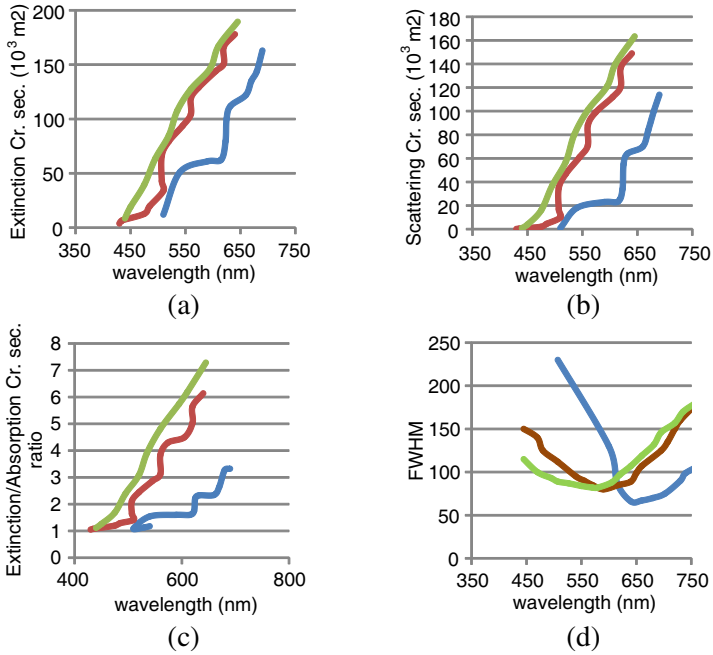

Figure 4. (a) Extinction, (b) scattering, (c) extinction/absorption cross section ratio, and (d) FWHM for a silver nano-triangle (blue), a silver nano-diamond (red), and a silver nano-sinusoid (green) vs. plasmon wavelength.

500 nm wavelengths, the nano-sinusoid and the nano-diamond absorb less energy (lower absorption cross section) with respect to the nano-triangle. Moreover, the nano-triangle exhibits a lower scattering cross section too. Consequently, the efficiency for the nano-diamond and the nano-sinusoid is higher. In particular, the nano-sinusoid exhibits the highest and more linear extinction and scattering cross section over the entire wavelength range of interest. Full in-plane width at half maximum (FWHM) is another important factor, giving an indication of the sharpness of the plasmon spectrum, i.e., damping mainly due to interband and intraband energy activation thresholds, which is strongly dependent on the shape and material of the NPs. Figure 4(d) compares the FWHM values for the three structures. This figure demonstrates extremely sharper plasmon spectrum for nano-sinuoids than nano-triangles in the visible wavelength less than around 615 nm; however, as the plasmon wavelength goes upper than this value, nano-triangles exhibit a sharper spectrum.

The effect of aspect ratio on dipole inverse eigenvalues of the NPs for an incident light polarized along the symmetry axis elongation (x-

axis in these simulations) for various minor axis sizes and NP thickness of 30 nm is shown in Figure 5. The relevant extinction cross sections are displayed in Figure 6. The graphs show the best linearity of the plasmon parameters with respect to aspect ratio for nano-sinusoids and the worst linearity for the nano-diamonds; nano-sinusoids have a mild and symmetric shape which prohibits the generation of multipoles. In addition, increasing the aspect ratio in the NPs enhances the surface plasmon electric fields on one hand, and red-shifts the dipolar plasmon

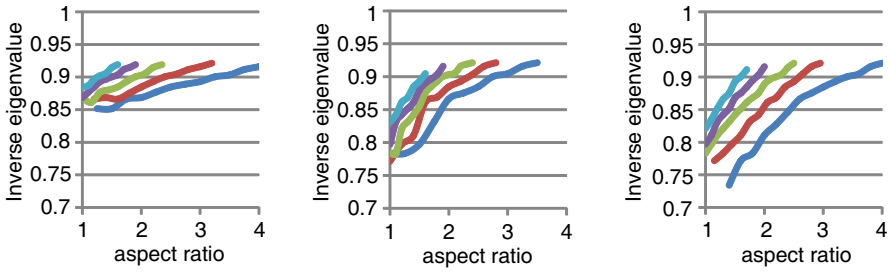

Figure 5. Dipolar inverse of eigenvalues for (a) nano-triangles, (b) nano-diamonds, and (c) nano-sinusoids vs. aspect ratio as a function of minor axis size of $w = [30, 45, 60, 75, 90]$ nm for nano-triangles, $w = [40, 60, 80, 100, 120]$ nm for nano-diamonds, and $w = [40, 60, 80, 100, 120]$ nm for nano-sinusoids displayed by colours [blue, red, green, purple, light blue] from the smallest to the largest.

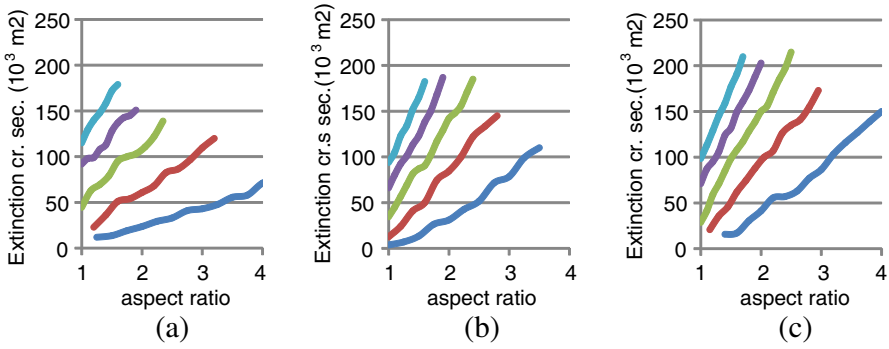

Figure 6. Dipolar extinction cross sections for (a) nano-triangles, (b) nano-diamonds, and (c) nano-sinusoids vs. aspect ratio as a function of minor axis size of $w = [30, 45, 60, 75, 90]$ nm for nano-triangles, $w = [40, 60, 80, 100, 120]$ nm for nano-diamonds, and $w = [40, 60, 80, 100, 120]$ nm for nano-sinusoids displayed by colours [blue, red, green, purple, light blue] from the smallest to the largest.

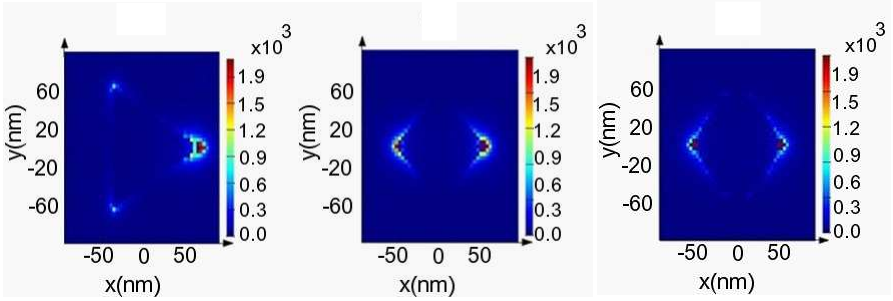

Figure 7. Total electrical field intensity on plane xy on the upper base ($z = 15$ nm) of (a) a nano-triangle with in-plane width of 112 nm and thickness of 30 nm, (b) a nano-diamond with in-plane width of 112 nm and thickness of 30 nm, and (c) a nano-sinusoid with in-plane width of 112 nm and thickness of 30 nm.

wavelength on the other hand. The larger the size of the minor axis (along y-axis) of each NP is, the steeper the ramp of enhancement and inverse-eigenvalue-growth become.

In addition, Figure 7 shows the plasmon electric field along the sharp tips of an equilateral nano-triangle, an equilateral nano-diamond, and a symmetric nano-sinusoid with the identical sizes of 112 nm and thickness of 30 nm, when illuminated by a plane wave polarized along the x-axis. As expected, for this polarization direction, more electric fields are collected along the x-axis (polarization direction) on the tips of both upper and lower bases of the NPs, i.e., surface plasmon electric fields are slowed down in the vicinity of the singularities resulting in more confined energy at the hot spots.

However, to the best of our knowledge some important issues, such as the divergent features of the structure and the influence of source location on the field enhancement, have not been discussed yet. the electric field diverges at the vertex (singularity) of the structure even when the material is highly dissipative. This divergent feature then disappears above a critical frequency; the electric field vanishes as surface plasmons propagate toward the vertex, whereas a considerable field enhancement is still expected along the metal surface.

The graphs demonstrate more surface electric fields on the tips of the nano-triangles than nano-diamonds and nano-sinusoids, and almost the same enhancement for the last two NPs.

4. CONCLUSION

An investigation on the spectral properties and the scattering characteristics of three different NPs in the visible frequency range

was carried out. The numerical analysis demonstrates the advantages of nano-diamonds and nano-sinusoids with respect to nano-triangles, since the first two NPs present two hot spots at the two end vertices, a wider range of applicable plasmon wavelength, and higher electric field enhancement for the same resonant wavelengths. Furthermore, increasing the NPs size or aspect ratio incurs more dipolar and less multipolar extinction and scattering cross sections, besides shifting the dipolar resonance towards red light. Moreover, nano-triangles and with a higher extent nano-diamonds exhibit more non-linearity in their plasmon spectrum-size relationship because of their higher singularities due to many sharp edges, which makes the engineering of their plasmon wavelength uncontrollable. The linear relationship is very essential in solving the plasmon interactions between the NPs and tuning the plasmon wavelengths for applications such as SERS biosensing using the electrostatic eigenmode interaction method. The nano-sinusoids shape introduced in this paper possess such characteristics, making it a valid alternative to other NPs. In addition, it was analytically demonstrated that the surface plasmon excitations have a lower bound cutoff at a finite frequency on singular structures; in addition, the electric field diverges below a critical frequency even when metallic losses are considered.

REFERENCES

1. Li, S., S. Yin, Y. Jiang, C. Yin, Q. Deng, and C. Du, "Specific protein detection in multiprotein coexisting environment by using LSPR biosensor," *IEEE Transactions on Nanotechnology*, Vol. 9, 554–557, 2010.
2. Sadeghi, S. M., "Plasmonic metaresonance nanosensors: Ultrasensitive tunable optical sensors based on nanoparticle molecules," *IEEE Transactions on Nanotechnology*, Vol. 10, 566–571, 2011.
3. Mortazavi, D., A. Z. Kouzani, and A. Kaynak, "Nano-plasmonic biosensors: A review," *ICMEA'11*, Harbin, China, 2011.
4. Willets, K. A. and R. P. van Duyne, "Localized surface plasmon resonance spectroscopy and sensing," *The Annual Review of Physical Chemistry*, Vol. 58, 267–297, 2007.
5. Haes, A. J. and R. P. van Duyne, "A nanoscale optical biosensor: Sensitivity and selectivity of an approach based on the localized surface plasmon resonance spectroscopy of triangular silver nanoparticles," *American Chemical Society*, Vol. 124, 10596–10604, 2002.
6. Mayergoyz, I. D., D. R. Fredkin, and Z. Zhang, "Electrostatic

(plasmon) resonances in nanoparticles," *Physical Review B*, Vol. 72, 155412–426, 2005.

7. Politano, A., et al., "Electronic properties of self-assembled quantum dots of sodium on Cu(111) and their interaction with water," *Surface Science*, Vol. 601, 2656–2659, 2007.
8. Politano, A., R. G. Agostino, E. Colavita, V. Formoso, and G. Chiarello, "High resolution electron energy loss measurements of Na/Cu(111) and H_2O/Na/Cu(111): Dependence of water reactivity as a function of Na coverage," *J. of Chemical Physics*, Vol. 126, 244712, 2007.
9. Slaughter, L., W. S. Chang, and S. Link, "Characterizing plasmons in nanoparticles and their assemblies with single particle spectroscopy," *J. Phys. Chem. Lett.*, Vol. 2, 2015–2023, 2011.
10. Angulo, A. M., C. Noguez, and G. C. Schatz, "Electromagnetic field enhancement for wedge-shaped metal nanostructures," *J. Phys. Chem. Lett.*, Vol. 2, 1978–1983, 2011.
11. Hao, F., C. L. Nehl, J. H. Hafner, and P. Nordlander, "Plasmon resonances of a gold nanostar," *Nano Letters*, Vol. 7, 729–732, 2007.
12. Richards, D., R. G. Milner, F. Huang, and F. Festy, "Tip-enhanced Raman microscopy: Practicalities and limitations," *J. of Raman Spectroscopy*, Vol. 34, 663–667, 2003.
13. Ishimaru, A., S. Jaruwatanadilok, and Y. Kuga, "Generalized surface plasmon resonance sensors using metamaterials and negative index materials," *Progress In Electromagnetic Research*, Vol. 51, 139–152, 2005.
14. Liu, X., J. Lin, T. F. Jiang, Z. F. Zhu, Q. Q. Zhan, J. Qian, and S. He, "Surface plasmon properties of hollow AuAg alloyed triangular nanoboxes and its applications in SERS imaging and potential drug delivery," *Progress In Electromagnetic Research*, Vol. 128, 35–53, 2012.
15. Zeman, E. J. and G. C. Schatz, "An accurate electromagnetic theory study of surface enhancement factors for silver, gold, copper, lithium, sodium, aluminum, gallium, indium, zinc, and cadmium," *J. of Chemical Physics*, Vol. 91, 634–643, 1987.
16. Schatz, G. C. and R. P. van Duyne, *Electromagnetic Mechanism of Surface-enhanced Spectroscopy*, John Wiley & Sons Ltd., Chichester, 2002.
17. Kelly, K. L., E. Coronado, L. L. Zhao, and G. C. Shatz, "The optical properties of metal nanoparticles: The influence of size, shape, and dielectric environment," *J. Physical Chemistry B*,

Vol. 107, 668–677, 2003.

18. Davis, T. J., K. C. Vernon, and D. E. Gómez, "Designing plasmonic systems using optical coupling between nanoparticles," *Physical Review B*, Vol. 79, 155423–155432, 2009.
19. Davis, T. J., D. E. Gomez, and K. C. Vernon, "Simple model for the hybridization of surface Plasmon resonances in metallic nanoparticles," *Nano Letters*, Vol. 10, 2618–2625, 2010.
20. Mortazavi, D., A. Z. Kouzani, A. Kaynak, and W. Duan, "Developing LSPR design guidelines," *Progress In Electromagnetic Research*, Vol. 126, 203–235, 2012.
21. Mortazavi, D., A. Z. Kouzani, and K. C. Vernon, "A resonance tunable and durable LSPR nano-particle sensor: Al_2O_3 capped silver nano-disks," *Progress In Electromagnetic Research*, Vol. 130, 429–446, 2012.
22. Mortazavi, D., A. Z. Kouzani, and A. Kaynak, "Investigating nanoparticle-substrate interaction in LSPR biosensing using the image-charge theory," *EMBC'12*, San Diego, USA, Aug. 2012.
23. Collin, R. E., *Foundations for Microwave Engineering*, Chapter 5, McGraw-Hill, New York, 1966.
24. Mortazavi, D., A. Z. Kouzani, and L. Matekovits, "Investigation on localized surface plasmon resonance of different nano-particles for bio-sensor applications," *ICEAA'12*, Cape Town, South Africa, 2012.
25. Kreibig, U. and M. Vollmer, *Optical Properties of Metal Clusters*, Springer, Berlin, Germany, 1995.
26. Zhou, X., M. Zhang, L. Yi, and Y. Fu, "Investigation of resonance modulation of a single rhombic plasmonic nanoparticle," *Plasmonics*, Vol. 6, 91–98, 2011.
27. Luo, Y., J. B. Pendry, and A. Aubry, "Surface plasmons and singularities," *Nano Letters*, Vol. 10, 4186–4191, 2010.
28. Taflove, A., *Computational Electrodynamics: The Finite-difference Time-domain Method*, Artech House, Boston, London, 1995.
29. Gao, C., Z. Lu, Y. Liu, Q. Zhang, M. Chi, Q. Cheng, and Y. Yin, "Highly stable silver nanoplates for surface plasmon resonance biosensing," *Angewandte Chemie*, Vol. 51, 5629–5633, 2012.
30. Link, S. and M. A. El-Sayed, "Spectral properties and relaxation dynamics of surface plasmon electronic oscillations in gold and silver nanodots and nanorods," *J. Physical Chemistry B*, Vol. 103, 8410–8426, 1999.